J Mater Sci (2007) 42:1444–1454
DOI 10.1007/s10853-006-0969-8

The effect of annealing on deformation and fracture of a nanocrystalline fcc metal

Fereshteh Ebrahimi · Hongqi Li

Received: 1 June 2006 / Accepted: 12 September 2006 / Published online: 13 January 2007

Abstract The tensile deformation and fracture behavior of electrodeposited nanocrystalline Ni–15% Fe alloy samples after annealing for 90 min at 250, 400 and 500 °C temperatures were investigated. The structure of the samples was studied using TEM and XRD techniques and the fracture surfaces were investigated employing SEM. The results of this study indicated that annealing at 250 °C modified grain size distribution slightly but resulted in a significant increase in the initial strain hardening rate. While the average grain size in the 400 °C sample was increased to 59 nm, its yield strength was comparable to the as-deposited alloy with a 9 nm grain size. The plastic tensile elongation of all annealed samples was lowered significantly to less than 1% from approximately 6% in the as-deposited state. These results are discussed in terms of the inhomogeneity of plastic deformation and the evolution of internal stresses in nanocrystalline materials.

Introduction

The mechanical properties of nanocrystalline metals have been the focus of many experimental and theoretical studies in the past two decades. These materials have ultra-high strength levels and recent experimental investigations have demonstrated that in the absence of processing defects they exhibit reasonable tensile elongation [1–4]. As the grain size is reduced within the nanoregime (conventionally assumed <100 nm), the generation of dislocations from inside the grains and the formation of pile-ups at boundaries become less probable and eventually the dislocation activity becomes limited to the motion of single dislocations generated from grain boundaries [5–7]. With the increased difficulty in dislocation motion and the rise in the grain boundary volume fraction, the grain boundary-mediated deformation mechanisms become possible at very small grain sizes [8–10]. Consequently, simulation results predict that at a critical grain size (approximately 10–20 nm for most metals) the strength of nanocrystalline materials decreases with a further refining of the grains [11–13] (also known as the inverse Hall–Petch relationship [5]). The rotation of grains through grain boundary mediated mechanisms has been confirmed in face-centered cubic (fcc) metals by in situ transmission electron microscopy (TEM) investigations [14, 15]. Furthermore, we have demonstrated that parallel to the deformation transition the fracture behavior of nanocrystalline fcc metals also goes through a ductile-to-brittle transition [16]. When dislocation activities are prevalent, fracture takes place by the conventional microvoid coalescence mechanism, designated as ''cup–cup'' behavior. However, at smaller grain sizes, although the fracture surface has a dimpled appearance, crack propagates intergranularly by breaking atomic bonds with a ''cup–cone'' behavior.

F. Ebrahimi (✉) · H. Li
Materials Science and Engineering Department,
University of Florida, Gainesville 32607, USA
e-mail: febra@mse.ufl.edu

Present Address:
H. Li
Department of Materials Science and Engineering,
University of Tennessee, Knoxville, TN, USA

Limited work has been conducted on the effect of annealing on deformation and fracture of nanocrystalline fcc metals. Weertman and Sanders [17] first demonstrated that low temperature annealing results in an increase in the hardness of nanocrystalline Pd. They attributed this effect to the relaxation of lattice strains as evidenced by X-ray studies. More recently, Wang et al. [18] have shown that annealing of an electrodeposited nanocrystalline Ni at 100 °C results in an increase in the tensile strength without a loss of tensile elongation. Annealing of this material at 150 °C increased the strength further but caused a reduction in the tensile elongation. The increase in strength was ascribed to the relaxation of grain boundaries which based on simulation results [19] makes grain boundary sliding as well as dislocation emission more difficult. Annealing above 200 °C resulted in pronounced grain growth and the samples fractured intergranularly within the elastic limit owing to the significant segregation of sulfur to grain boundaries. Hardening upon annealing at low temperatures has also been reported in severely deformed ultra-fine grained fcc metals, where grain boundary sliding is not prevalent. It has been suggested that reducing the density of dislocations is responsible for the increase in strength after annealing in such materials [20, 21].

The aim of this study was to investigate the effect of annealing temperature on deformation and fracture of a nanocrystalline Ni–15%Fe alloy. We have been successful in fabricating high quality nanocrystalline Ni–Fe alloys with no additives (less than 100 ppm sulfur), which allows investigating the annealing effect without the interference from the increased concentration of sulfur at grain boundaries upon grain growth [22, 23]. Furthermore, the addition of iron to nickel makes it possible to maintain the nanocrystalline structure after annealing at temperatures as high as 400 °C [24].

Experimental procedures

Ni–15wt%Fe alloy was deposited using a rotating disc electrode set-up and a nickel sulfumate plating bath. Details of the deposition procedure can be found elsewhere [22, 23]. The alloy was deposited on a copper substrate disc with a 35 mm diameter. The nominal thickness of deposits was 35 μm. After deposition, each disc was cut into four rectangular strips (approximately 24 mm × 6 mm) and the copper substrate was dissolved using a commercial copper-stripper.

Dog-bone shaped tensile specimens with a 3 mm width and a 5 mm gage length were hand-ground from the as-deposited alloy strips. The tensile specimens were encapsulated in glass tubes filled with argon and then annealed in a preheated box furnace. The heat treatment was conducted at 250, 400 and 500 °C for 90 min. This procedure did not cause any oxidation or discoloration of the samples.

Tensile testing was conducted at a nominal strain rate of 4.2×10^{-3} s^{-1} using an Instron mechanical testing system at room temperature. At least two samples were tested per condition. The samples were gripped using serrated pneumatic grips. Annealed copper lining was used in the shoulder area to avoid damage by the serrated jaws as well as to enhance the grip action due to the plastic deformation of the copper inserts. Scanning electron microscopy (SEM) was employed to accurately measure the thickness of individual samples and investigate their fracture behavior. The grain size was evaluated by X-ray diffraction (XRD) as well as TEM techniques. A Philips APD 3720 X-ray diffractometer in conjunction with the Line Profile program was applied to measure the grain size and the lattice strain using the (111) peak. Thin foils were prepared by jet polishing and were studied in JEOL 200CX microscope for grain size distribution measurements. The high magnification TEM studies were conducted in a JEOL 2010F microscope.

Results

Structural analysis

Previous studies have revealed that the Ni–Fe alloy deposits used in this investigation are composed of a single fcc phase with a close to random crystallographic orientation [22]. The composition has been shown to be homogeneous through the thickness as well as along the radius of the discs. Figures 1 and 2 present the microstructure of the Ni–15%Fe alloy in as-deposited and annealed states, respectively. No phase separation or ordering was detected in the annealed microstructures. The grains in both as-deposited and annealed samples were heavily twinned. Figure 1b presents a high magnification TEM micrograph showing extensive growth twins in the as-deposited alloy. Figure 1c exhibits a high resolution TEM picture of a twin in this material. Twins can also be resolved in TEM micrographs given in Fig. 2, particularly in the larger grains.

The results of lattice strain and grain size measurements are presented in Table 1. The average grain size calculated from the TEM analysis is reported in terms

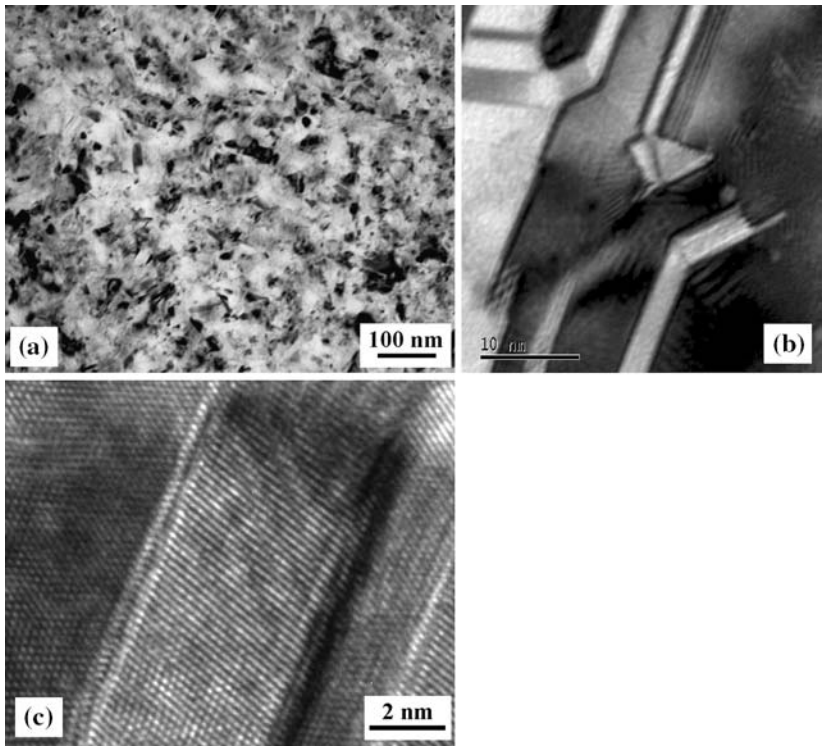

Fig. 1 TEM micrographs showing (**a**) the general grain structure, (**b**) a high density of twins, and (**c**) the twin structure at a high resolution in the as-deposited Ni–15%Fe alloy

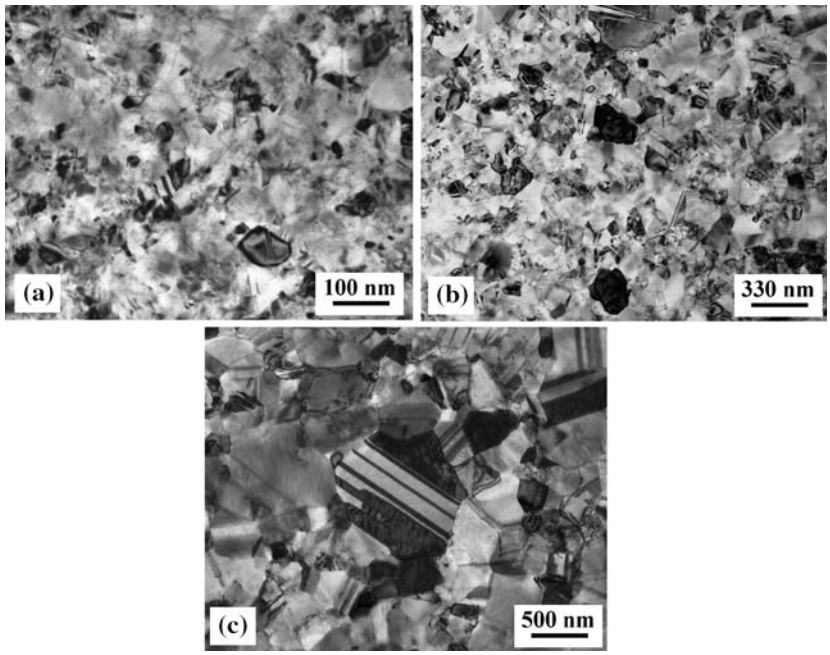

Fig. 2 TEM micrographs of samples annealed for 90 min at (**a**) 250 °C, (**b**) 400 °C and (**c**) 500 °C

of both number frequency and volume fraction. Owing to the significant contribution of the large grains to the volume fraction, the average grain size calculated based on volume fraction is larger than the value obtained based on the number frequency. The XRD results are anticipated to reflect the relative volume fraction of the grains, however, the lower values obtained in comparison to the TEM results can be attributed to the presence of twins in the structure. Due to the large grain size, reproducible values could not be measured for the 500 °C annealed sample using XRD. Annealing at 250 °C increased the average grain size slightly and caused very limited abnormal grain growth. Extensive grain growth took place upon

Table 1 Lattice strain and grain size measurements

sample	Lattice strain (%)	Grain size (nm)		
		XRD	TEM[a]	TEM[b]
As-deposited	0.208	12	9	17
250 °C	0.106	14	11	62
400 °C	0	66	59	152
500 °C	–	–	278	559

[a] Average grain size based on the number frequency

[b] Average grain size based on the volume fraction

annealing at 500 °C for 90 min but the average grain size remained within the nanoregime after annealing at 400 °C. These two temperatures resulted in a bimodal grain size distribution as can be seen in the TEM pictures presented in Fig. 2b and c. Figure 3 shows the grain size distributions for the samples annealed at 400 and 500 °C and they demonstrate that the bimodal behavior is best detected when the grain size distribution is presented as the relative volume fraction of grains.

Significant drop in the lattice strain was found after annealing at 250 °C. This decease in the lattice strain is partially associated with the relaxation of grain boundaries as reported previously [17]. No lattice strain was measured for samples annealed at higher temperatures. Figure 4 presents the (111) XRD peaks for the Ni–15%Fe alloy for different heat treating conditions. In addition to the loss of line broadening with increasing the annealing temperature, there is a noticeable shift in the peak position after annealing at 500 °C. This observation suggests that the samples were under residual stresses, which were then released after annealing at this temperature. We attribute this behavior to the interconnectivity of large grains after annealing at 500 °C. In contrast, in the 400 °C annealed samples, the large annealed grains are separated by the finer grains, which their high strength inhibits the complete relaxation of the residual stresses.

Tensile properties

A summary of tensile tests results is given in Table 2. Figure 5 shows typical stress–strain curves for as-deposited as well as annealed samples. Note that strain was measured based on the cross-head speed and consequently the slope of the linear portion of the curves does not reflect the true elastic modulus.

All samples fractured after yielding. Annealing at 250 °C caused an increase in yield strength (0.2% offset) but the strength was reduced in samples heat treated at higher temperatures. It is interesting to note that the 400 °C annealed sample with an average grain size of 59 nm showed a yield strength comparable to that of the as-deposited sample with an average grain size of 9 nm. Figure 6 presents the yield strength as a function of the inverse of square root of grain size

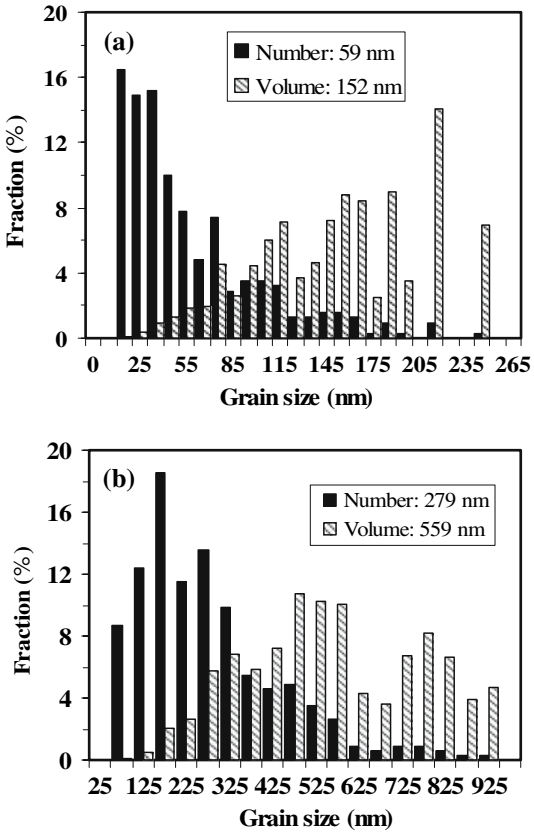

Fig. 3 Grain size distribution for samples annealed at (**a**) 400 °C and (**b**) 500 °C

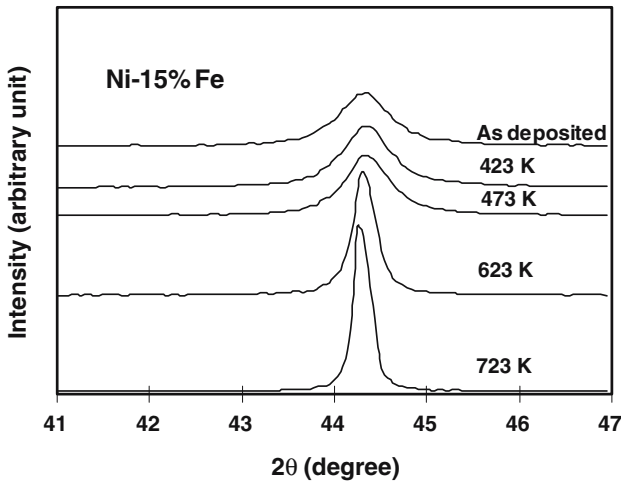

Fig. 4 (111) XRD peak for the Ni–15%Fe alloy in as-deposited and annealed conditions

Table 2 A summary of tensile results

Sample	Yield strength (MPa)	Tensile strength (MPa)	Plastic elongation (%)
As-deposited	1,634	2,326	6.00
	1,540	2,386	5.60
250 °C	1,812	2,417	1.70
	1,880	2,295	0.55
400 °C	1,476	1,916	0.76
	1,420	1,669	0.40
500 °C	1,027	1,170	0.45
	1,004	1,060	0.30
	1,110	1,234	0.33
	1,213	1,289	0.29

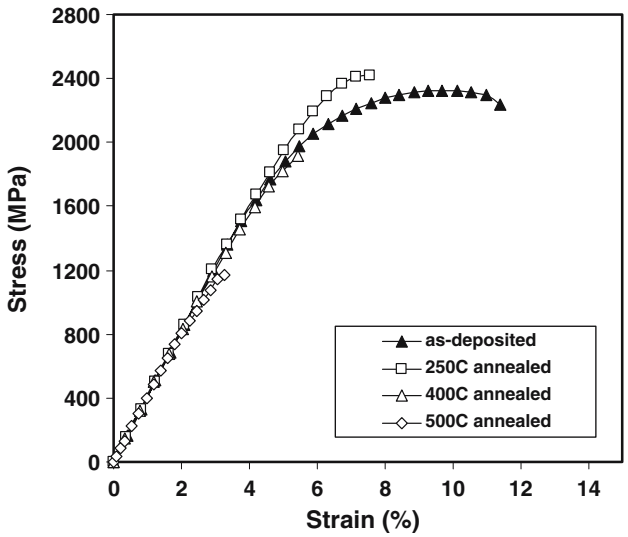

Fig. 5 Typical tensile engineering stress–strain curves for the Ni–15%Fe alloy samples tested

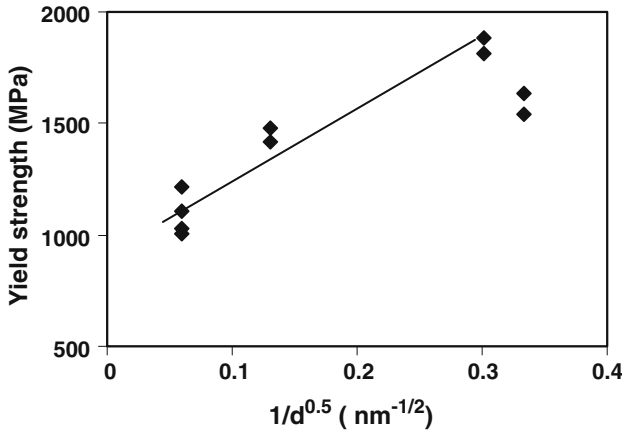

Fig. 6 Hall–Petch plot showing the linear relationship among the annealed samples

($1/d^{0.5}$). The results suggest that among the annealed samples, the yield strength follows the Hall–Petch relationship, i.e. increases linearly with the inverse of the square root of grain size.

Annealing resulted in a significant loss of tensile elongation. While the stress–strain curves of the as-deposited alloy showed tensile instability, i.e. $dP = 0$ (P = load) [25], the annealed samples fractured prematurely without any post-uniform elongation. Since the very low tensile elongation of the 500 °C annealed samples was surprising, we repeated the test for ascertaining the validity of the results (see Table 2). For a given annealing condition, some variations in the tensile elongation and hence the fracture stress values were observed. However, consistently fracture occurred after yielding and the engineering fracture stress values, which correspond to the tensile strengths in the case of annealed samples, decreased with increasing the annealing temperature.

Fracture behavior

The fracture behavior of the as-deposited Ni–15%Fe alloy has been discussed elsewhere [16, 25]. These studies have shown that the tensile samples of as-deposited alloy break with a limited reduction in area except in the shear lip sections where the stress-state changes to a plane-stress condition. In these samples, tensile failure takes place by formation of microcracks that join each other and create large steps on the fracture surface. Relatively large and distinct plastic zones are associated with these microcracks. Further investigation has revealed that in the as-deposited samples crack grows intergranularly along a microscopic path that creates cup-cone features on the matching fracture surfaces. It has been concluded that extensive plasticity precedes the fracture of as-deposited Ni–15%Fe samples, but the mechanism of fracture is brittle and it happens by breaking atomic bonds.

Figure 7 presents SEM pictures from the fracture surface of a 250 °C annealed sample. Figure 7b was magnified from the squared area shown in Fig. 7a. Sections of the sample fractured with no noticeable area reduction as shown in Fig. 7a. Two regions, which appear bright and dark, are distinguishable on the fracture surface of these sections. The higher magnification picture (Fig. 7b) clearly shows that the darker regions are associated with considerable shearing, while the brighter regions have a void-like morphology, similar to features observed on the fracture surface of the as-deposited material. The size of these void-like features is much larger than the grain size of this material. The necking was inhomogeneous through

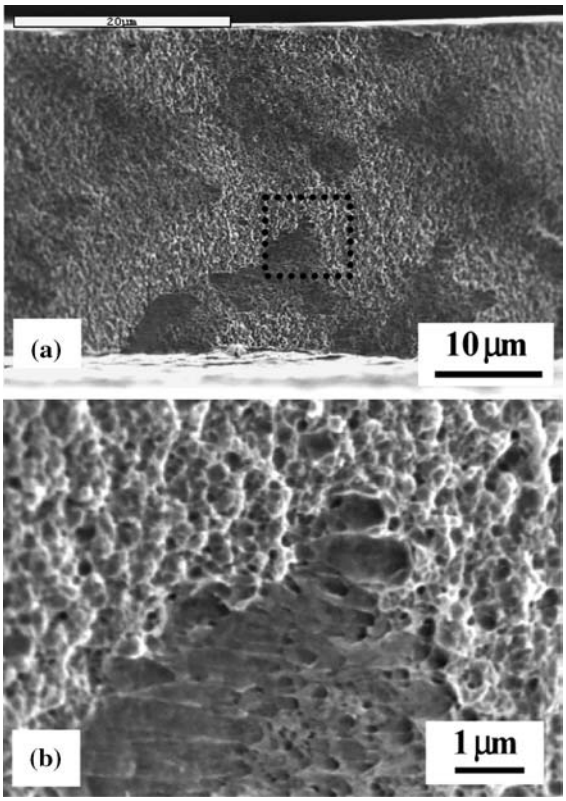

Fig. 7 SEM pictures from the fracture surface of a 250 °C annealed sample showing (**a**) limited area reduction in a section and (**b**) the extensive shearing in the dark regions seen in (**a**)

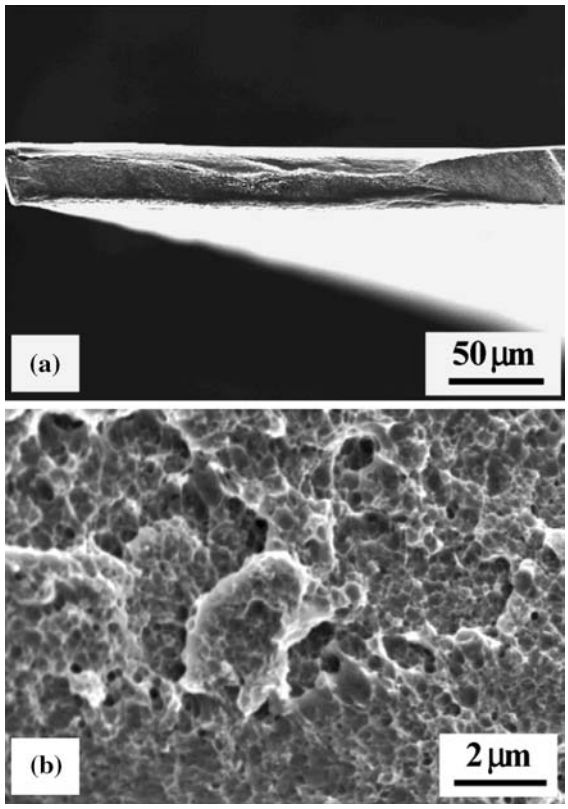

Fig. 8 SEM pictures from a 250 °C annealed sample showing (**a**) inhomogeneous necking along the width of a sample and (**b**) the observation of more plasticity associated with the sections with extensive necking

the width of the sample. As shown in Fig. 8a, there were sections that exhibited extensive necking. The fracture surface was much rougher with deeper void-like features in these sections as shown in Fig. 8b.

The fracture profiles for a 400 °C annealed sample are presented in Fig. 9. Similar to the as-deposited and 250 °C annealed samples, fracture proceeded by microcracking that resulted in slip marks on the sample surfaces and large steps on the fracture surface. Figure 10 demonstrates that the two distinct dark and bright regions also developed in this sample. However, the percent of the darker regions, which formed under sever shearing, increased in comparison to the 250 °C annealed sample. The void-like features are much larger than the grain size of this material, but they showed a size distribution reflective of the heterogeneity of the microstructure of this material.

The 500 °C annealed material exhibited significant necking (Fig. 11a), whose extent varied along the width of the samples. These samples did not show any brittle fracture and most probably failed by the microvoid coalescence mechanism as shown in Fig. 11b. Consistently, the depth of the voids correlated with the degree of necking, i.e. deeper voids were found in the extensively reduced areas. The absence of intergranular fracture in these samples confirms the low level of impurities in the deposited Ni–15%Fe alloy studied here. Therefore, the low tensile elongation of this sample cannot be attributed to an embrittlement phenomenon.

All annealed samples were prone to strain localization. The 250 and 400 °C annealed samples behaved similar to the as-deposited samples, where microcracks developed internally in the samples. As these microcracks propagated toward the surface, their plastic zones arrived on the surface first, resembling a band of plastic localization [25]. Figure 12a shows the formation of such a band in a 250 °C annealed sample. In this picture, the features seen on the surface (three of such features are marked by arrows) correspond to the strain localization resulting from the plastic zone of subsurface microcracks. Interestingly, this sample fractured at a different point, suggesting that the localization can occur in more than one section. Figure 12b presents the side profile of a 500 °C annealed sample. In this picture it is obvious that a deposition defect (marked A) caused the strain localization but the fracture proceeded on another favorable path. It

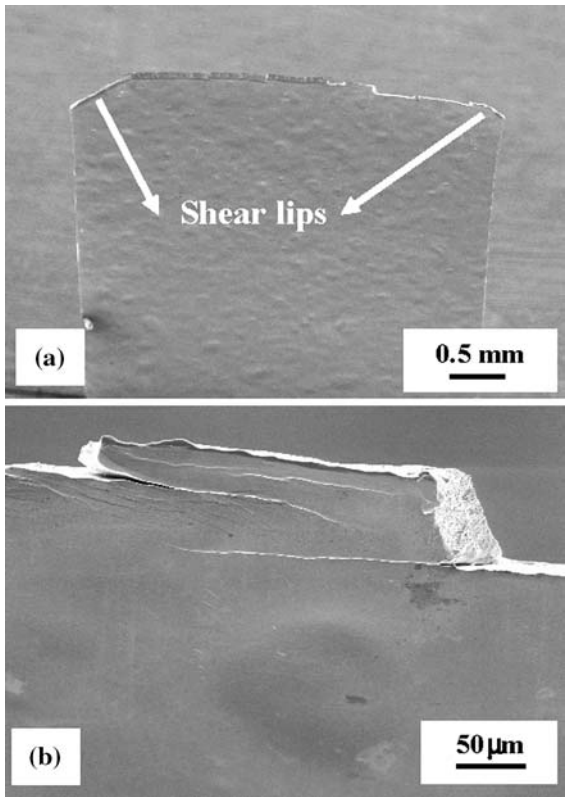

Fig. 9 SEM pictures showing (**a**) the general crack profile and (**b**) the formation of microcracks that lead to the development of steps on the fracture surface of a 400 °C annealed sample

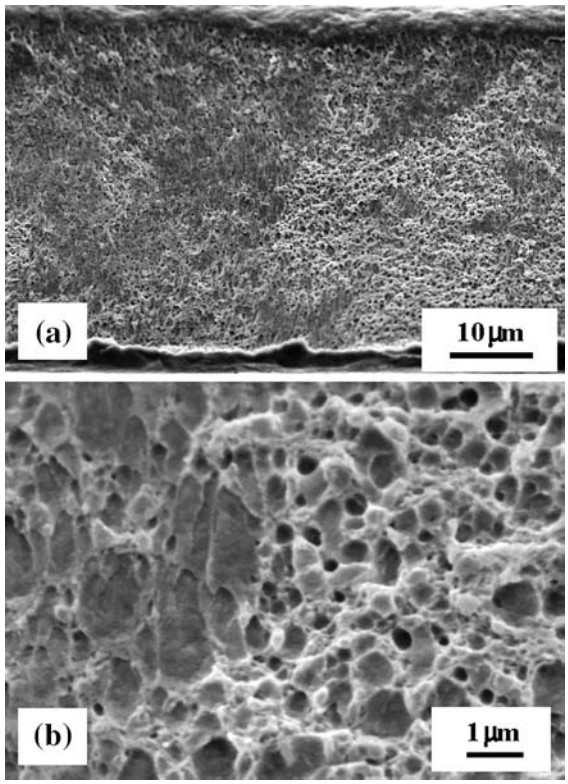

Fig. 10 SEM pictures showing (**a**) the large percent and (**b**) the shear nature of the dark regions on the fracture surface of a 400 °C annealed sample

should be noted that no microcracking was found in the 500 °C annealed sample and the strain localization observed was associated with plastic instability.

Discussion

It is well accepted that in nanocrystalline as well as in ultra-fine grained metals dislocations are generated from grain boundaries. Molecular-dynamics (MD) simulations of columnar grain structures, where dislocations are constrained to be straight, have shown that the dislocation nucleation stress is independent of grain size [26]. Consistently, the results of three-dimensional MD simulation of tensile testing of nanocrystalline copper with different grain sizes [27] also suggest that the dislocation nucleation stress is not very sensitive to the grain size as long as grain boundary sliding is not prevalent, as evidenced by the insensitivity of the upper yield point at grain sizes above approximately 25 nm. Indeed these results indicate that the initial yield strength continuously decreases with lowering the average grain size within 5–50 nm range. However, the decrease in strength is most pronounced at small average grain sizes where grain boundary mediated deformation processes prevail. However, the average flow stress (7–10% strain) exhibits a maximum as a function of grain size, indicating that when grain boundary mediated mechanisms do not play a significant role in deformation, the motion of dislocations subsequent to their nucleation becomes more difficult in smaller grains. Considering that dislocations have to bow while emerging out of the grain boundaries, a dislocation generation stress has been defined which approximately varies inversely with the grain size [28]. In this model a semicircular dislocation configuration, similar to a Frank-Read source is assumed and the approach does not include the effect of grain boundary structure on the dislocation bowing. On the other hand, a model based on the confined motion of dislocations between two interfaces can incorporate the effect of the boundary structure on the dislocation bowing radius [7]. Usually, when dislocation generation is the controlling mechanism, the stress–strain curve exhibits the yield point phenomenon [28, 29]. However, we did not observe an upper yield point in our stress–strain curves. The absence of an upper yield point in the

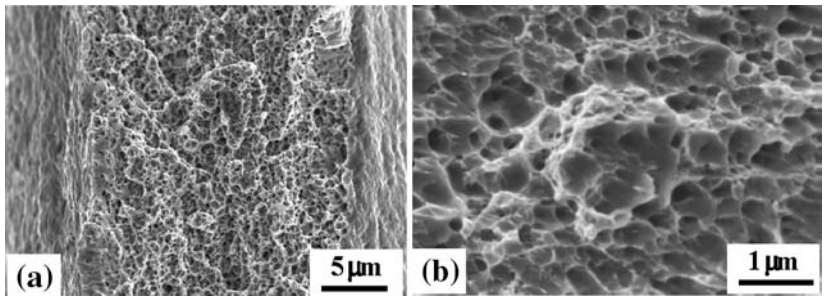

Fig. 11 SEM pictures showing (**a**) significant necking and (**b**) microvoid coalescence fracture behavior in a 500 °C annealed sample

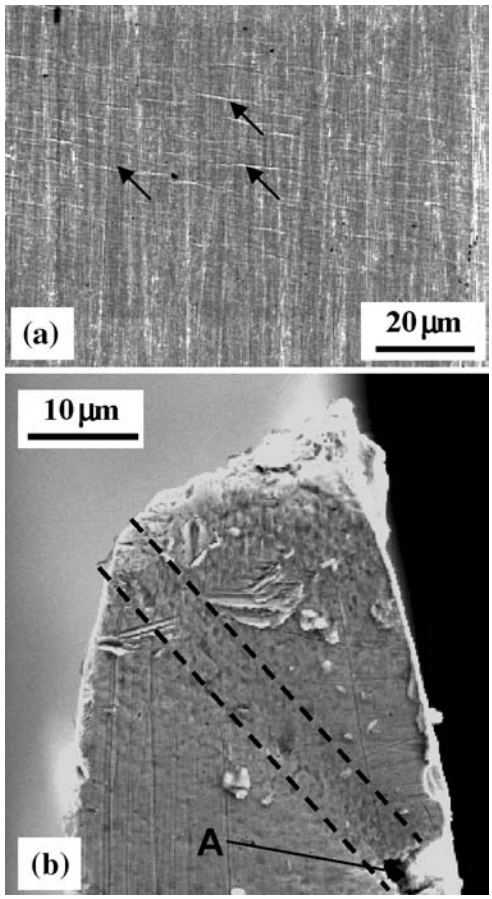

Fig. 12 Examples of strain localization in (**a**) 250 °C and (**b**) 500 °C annealed samples

as-deposited samples can be attributed to the dominance of the grain boundary mediated deformation processes, consistent with the MD results [27]. On the other hand, the annealed samples fractured after less than 1% plastic strain, and hence it is not clear whether the stress would have dropped with further plasticity. In addition to the stress required to generate and move dislocations, as discussed below, the development of internal stresses also play important roles in governing the initial strain hardening, the 0.2% off-set strength (yield strength) and fracture behavior of the nanocrystalline metals.

Considering the generation and motion of single bowed dislocations within nano-grains several facts need be considered for discussing the results of this study. In conventional coarse grained metals dislocation motion does not start simultaneously in all grains owing to elastic and plastic anisotropy. In nanocrystalline metals, this inhomogeneity in plastic deformation is strongly amplified by the fact that due to the grain size distribution, the stress required to cause plastic deformation varies significantly among the grains. Furthermore, when a dislocation moves in a nanograin it creates a much larger local shear strain than it does in a micrograin. The level of local shear strain, γ, achieved by the motion of one dislocation in one grain is of the order of b/d (according to Orowan equation $\gamma = NbA$, N is the #dislocations per unit volume, b the Burgers vector, A the area sheared; for one dislocation: $N = 1/d^3$, $A = d^2$, $\gamma = b/d$). For example, assuming $b = 0.3$ nm the local shear strain will be of the order of 2 and 0.02% for grains of $d = 15$ nm and $d = 1.5$ μm, respectively. The heterogeneity of deformability of grains can be modeled similar to a composite material [30, 31]. The nanocrystalline structure can be envisioned as consisting of plastically deforming grains (soft grains) and elastically deforming grains (hard grains). The strain incompatibility between the plastically and elastically deforming grains creates large internal stresses, which retard the deformation of soft grains and encourage the deformation of hard grains [32]. Another important fact regarding the plastic deformation of nanocrystalline metals is that most plastic grains deform on less than five independent slip systems. Although this behavior is not mentioned explicitly in papers discussing simulation results, it can be deducted from the reported figures. Therefore, in a cluster of plastically deforming grains, additional internal stresses develop because of the lack of fulfillment of the Von Mises' criterion, which requires the activation of five independent slip systems for a general shape change [33]. We propose that the above

mentioned internal stresses, which develop due to strain incompatibilities, contribute significantly to the mechanical response of nanocrystalline metals.

In the absence of diffusion, dislocation cross-slip is the main recovery mechanism in coarse-grained metals and responsible for the decrease in the strain hardening rate with increasing the applied strain. In nanocrystalline materials, the probability of dislocation cross-slip is small and therefore other explanations for recovery processes are needed. In contrast to the composite materials, where the fraction of harder phase remains constant during deformation, in nanocrystalline materials as stress is increased a larger fraction of grains deform plastically with applied strain [31]. This decrease in the fraction of hard grains with applied strain will manifest as a reduction in the strain hardening rate.

The composite model of deformation of nanocrystalline metals, consistent with experimental results, predicts that strain hardening rate increases with decreasing the average grain size and tightening of the grain size distribution [30, 31]. However, in materials with very small average grain sizes (less than the so-called critical grain size), the grain boundary mediated deformation processes such as grain boundary sliding contribute to the relief of the internal stresses caused by strain incompatibility and act as recover processes. The proposed decrease in the strain hardening rate with reducing grain size beyond the critical grain size is consistent with theoretical predictions of reduced flow stress [27], creep rate [26] and susceptibility to nanocracking [34].

Based on the discussions presented above now we will consider the effect of annealing on the deformation and fracture of the Ni–15%Fe alloy. Annealing at 250 °C eliminated most of the lattice strain by modifying the grain boundaries without a significant change in the grain size distribution. Our results indicate that the initial strain hardening in these samples was increased significantly in comparison to the as-deposited material. The relaxation of grain boundaries upon annealing can result in a higher yield strength and strain hardening rate by several mechanisms. As far as dislocation generation and motion is concerned, not only the emission of dislocations from relaxed boundaries becomes more difficult [19] but also a change in the grain boundary structure may retard the motion of dislocations. Considering that the two ends of a dislocation moving in a grain are pinned by the boundaries with the adjacent grains [7], a change in the structure of the boundaries can enhance the pinning effect and increase the strength by increasing the curvature of the moving dislocations [31]. Furthermore, the relaxation of grain boundaries limits the grain boundary mediated deformation processes [19], which as discussed earlier, will diminish the recovery of internal stresses in nanocrystalline materials and consequently increase the strain hardening rate.

The average grain size grew considerably after annealing at 400 °C, but in comparison to the as-deposited sample the yield strength and the initial strain hardening rate did not change significantly. The larger grain size in this material is expected to significantly reduce the stress required for dislocation bowing [7, 27] and hence result in a lower strength. On the other hand, there are other mechanisms to compensate for the anticipated drop in strength. In addition to the mechanisms presented for the 250 °C annealed sample, the loss in grain boundary area due to the grain growth reduces the density of dislocation sources [35] and hence makes the dislocation generation process less accessible in the 400 °C annealed samples. The grain size heterogeneity can also contribute to the high strength of this material. As demonstrated in Fig. 3a, this material showed a wide grain size range with large grains being surrounded by very small grains (Fig. 2). In such a structure, although the larger grains can deform plastically at much smaller stress levels, the surrounding smaller grains control the deformation. This structure can be compared to a hard material which contains a distribution of soft particles [36]. As long as the soft phase is isolated and not interconnected the apparent yielding will be controlled by the hard interconnected phase. Therefore, the plastic deformation in 400 °C annealed material is governed by the dislocation activities in the finer grains, which require higher stresses.

Annealing at 500 °C resulted in significant grain growth and noticeable reduction in yield strength. Obviously the larger grain size makes the dislocation generation and motion much easier. Another factor that may contribute further to the low yield strength is the grain size distribution. In contrast, to the microstructure of the 400 °C annealed samples, in this material larger grains are interconnected and the smaller grains are isolated, as evidenced by the release of residual stresses (see Fig. 4). In this case, the applied strain is accommodated by the interconnected larger grains which require less stress for dislocation generation and motion.

It should be noted that while the yield strength of the annealed samples exhibited a Hall–Petch relationship the explanation of this behavior is not straightforward and includes many processes that control dislocation generation and load distribution among the grains of various sizes.

All samples fractured after yielding revealing that plasticity is necessary for crack initiation. In as-deposited nanocrystalline Ni–15%Fe alloy with 9 nm average grain size, the ability to relieve internal stresses by grain boundary mediated deformation inhibits nanocracking at grain boundaries and triple junctions, and hence the material continues to work harden through the activation of slip in smaller grains and new slip systems in the larger grains. Consequently, in this material plastic instability preceded fracture and a reasonable tensile elongation was achieved [25]. Annealing resulted in a considerable loss of tensile elongation but promoted necking, which was quite inhomogeneous along the width of each tensile specimen. We have previously reported the pre-mature fracture of fcc nanocrystalline electrodeposits with significant necking and reduction in area [37–40]. In as-deposited materials this phenomenon was attributed to the presence of defects or the co-deposition of hydrogen during electrodeposition. However, in the annealed samples studied here these explanations are not relevant.

The 250 and 400 °C annealed samples fractured by the formation of brittle microcracks, similar to the as-deposited samples. Therefore their low tensile elongation is associated with the ease of brittle crack formation. In comparison to the as-deposited material, the lack of grain boundary mediated deformation mechanisms is expected to reduce the applied strain necessary for crack initiation in these samples. In other words, due to the absence of recovery processes, large enough local stresses are achieved with a lower level of dislocation activity (i.e. applied strain). The presence of two distinct fracture regions in these samples (Figs. 7, 10) suggests that first fracture took place in a brittle manner in the ''lighter'' regions and then the ''darker'' regions were sheared. We have previously shown that the stress-state plays an important role in fracture of nanostructured metals [39, 40]. Plane-stress condition facilitates the propagation of plasticity by reducing constraint and results in a ductile fracture behavior. Therefore, it is reasonable to assume that the ligaments left between the brittle microcracks experience a plane-stress condition and shear extensively prior to fracture. This process is analogous to the formation of ''tearing ridges'' during fracture of conventional metals such as steels [42].

While the crack was initiated in a brittle manner in the 250 and 400 °C annealed samples, they showed a tendency to localized plastic deformation as evidenced by the observation of the ''dark'' sheared regions on the fracture surfaces and the presence of multiple necks along the width of some samples. The tendency to strain localization was further increased in the 500 °C annealed samples, which did not exhibit any brittle fracture. These samples failed in a ductile manner with extensive reduction in area but very limited tensile elongation. In the absence of embrittlement mechanisms, brittle cracks can develop in fcc metals if the local stresses are intensified significantly. The lack of brittle fracture indicates that the very high internal stresses required did not develop in this material. This behavior is suggested to be associated with the extensive grain growth after annealing at 500 °C. As was explained previously, the motion of single dislocations creates much smaller local shear strains in larger grains. Furthermore, the probabilities of multiple slip system activation and cross-slip are anticipated to be higher in larger grain sizes.

The increased propensity of the annealed samples to shear localization may be attributed to the inhomogeneity of their deformation. Due to the low dislocation density of the electrodeposited nanocrystalline metals, it is reasonable to assume that plastic deformation is initiated by generation of dislocations at several points in a tensile sample. With further straining, the accumulation of internal stresses will eventually cause either fracture or dislocation generation and motion in the adjacent grains. Because of the considerable inhomogeneity of the microstructure this process most probably takes place in a localized manner. In the absence of brittle fracture, the deformation band or (Lüders band) may either traverse the length of the sample or cause localized necking that will eventually lead to ductile fracture. Low strain rate sensitivity and localized softening propel the latter behavior. It should be noted that the presence of a bimodal grain size distribution does not necessarily imply a tendency to localization. Indeed it has been shown that when dislocation generation is not an issue, a bimodal grain size distribution improves the maximum uniform strain by increasing the strain hardening rate [41]. In these materials, because of their processing methods they have plenty of dislocations and intragranular dislocation sources; hence plastic deformation is not expected to be inhomogeneous. Consistently, it has been demonstrated that introduction of dislocations to an ultra-fine grained annealed aluminum sample restores the tensile elongation [20]. While lack of mobile dislocations is not sufficient to result in low tensile elongation (e.g. mild steels), it enhances the susceptibility to strain localization (e.g. stretch marks on sheet mild steel). Further work is needed to prove that indeed a combination of low dislocation density and a heterogeneous microstructure is needed for premature necking.

Conclusions

The tensile deformation and fracture of an electrodeposited nanocrystalline Ni–15%Fe alloy with a very low concentration of sulfur (<100 ppm) in as-deposited and annealed states (250, 400 and 500 °C for 90 min) were investigated. The results of this study led to the following conclusions:

1. Annealing at 250 °C caused an increase in the initial strain hardening rate and consequently yield strength. This behavior is attributed to the reduced abilities for dislocation emission and grain boundary mediated deformation processes, which enhance the development of local internal stresses and limit the recovery of them. The yield strength followed a Hall–Petch relationship among the annealed samples.
2. All samples tested fractured after yielding, suggesting that plastic deformation is necessary for crack initiation and propagation. The development of internal stresses due to plastic strain incompatibility is suggested to be responsible for brittle crack initiation.
3. Annealing resulted in a significant loss of tensile elongation. In the 250 and 400 °C annealed samples crack was initiated in a brittle manner. Their low tensile elongation can be ascribed to the rapid accumulation of internal stresses which reduce the applied strain needed for crack initiation. In comparison, the grain boundary mediated processes in the as-deposited material relieve the internal stresses and hence plastic instability precedes fracture.
4. The annealed materials were susceptible to strain localization, which manifested as inhomogeneous necking along the width of each tensile specimen and the low tensile elongation of the 500 °C annealed samples. This behavior was attributed to the inhomogeneity of the microstructure of annealed materials.

Acknowledgements Financial support for this research was provided by the National Science Foundation under the grant DMR-9980213 and DMR-0605406.

References

1. Karimpour AA, Erb U, Aust KT, Plaumbo G (2003) Scripta Mater 49:651
2. Li H, Ebrahimi F (2004) Appl Phys Lett 84:4307
3. Shen YF, Lu L, Lu QH, Jin ZH, Lu K (2005) Scripta Mater 52:989
4. Youssef KM, Scattergood RO, Murty KL, Horton JA, Koch CC (2005) Appl Phys Lett 87:929
5. Nieh TG, Wadsworth J (1991) Scripta Metall Mater 25:955
6. Lian J, Baudelet B, Nazarov AA (1993) Mater Sci Eng 172:23
7. Embury JD, Hirth JP (1994) Acta Metall Mater 42:2051
8. Chokshi AH, Rosen A, Karch J, Gleiter H (1989) Scripta Metall 23:1679
9. Milligan WW, Hackney SA, Ke M, Aifantis EC (1993) Nanostruct Mater 2:267
10. Hahn H, Padmanabhan KA (1997) Philos Mag 76:559
11. Schiøtz J, Di Tolla FD, Jacobsen KW (1998) Nature 391:561
12. Van Swygenhoven H, Spaczer M, Caro A (1999) Acta Mater 47:3117
13. Yamakov V, Wolf D, Phillpot SR, Mukherjee AK, Gleiter H (2003) Philos Mag Lett 83:385
14. Ke M, Hackney SA, Milligan WW, Aifantis EC (1995) Nanostruct Mater 5:689
15. Shan Z, Stach EA, Wiezorek JMK, Knapp JA, Follstaedt DM, Mao SX (2004) Science 305:654
16. Li H, Ebrahimi F (2005) Adv Mater 17:1969
17. Weertman JR, Sanders PG (1993) Solid State Phenom 35–36:249
18. Wang YM, Cheng S, Wei QM, Ma E, Nieh TG, Hamza A (2004) Scripta Mater 51:1023
19. Hasnaoui A, Van Swygenhoven H, Derlet PM (2002) Acta Mater 50:3927
20. Huang X, Hansen N, Tsuji N (2006) Science 312:249
21. Ma E, Shen TD, Wu XL (2006) Nature Mater 5:515
22. Li H, Ebrahimi F (2003) Acta Mater 51:3905
23. Li H, Ebrahimi F (2003) Mater Sci Eng A347:93
24. Ebrahimi F, Li H (2006) Scripta Mater 55:263
25. Li H, Ebrahimi F (2006) Acta Mater 54:2877
26. Yamakov V, Wolf D, Salazar M, Phillpot SR, Gleiter H (2001) Acta Mater 49:2713
27. Cheng S, Spencer JA, Milligan WW (2003) Acta Mater 51:4505
28. Schiøtz J, Jacobsen KW (2003) Science 301:1357
29. Johnston WG, Gilman JH (1959) J Appl Phys 30:129
30. Mitra R, Ungar T, Morita T, Sanders PG, Weertman JR (1999) In: Chung Y-W et al (eds) Advanced materials for 21st century: the 1999 Julia Weertman symposium. TMS Publication, Warrendale Pacific, p 553
31. Ebrahimi F, Ahmed Z, Morgan KL (2001) MRS Proc 634:B2.7.1
32. Tomota Y, Huroki K, Mori T, Tamura I (1976) Mater Sci Eng 24:85
33. Dieter GE (1986) Mechanical metallurgy, 3rd edn. McGrow-Hill, New York, p. 187
34. Ovi'ko IA, Sheinerman AG (2004) Acta Mater 52:1201
35. Espinosa HD, Berbenni S, Panico M, Schwarz KW (2005) Proc Nat Acad Sci 102:16933
36. Evans AG, Hirth JP (1992) Scripta Metall Mater 26:1675
37. Ebrahimi F, Zhai Q, Kong D (1998) Scripta Mater 39:315
38. Ebrahimi F, Bourne GR, Kelly MS, Matthews TE (1999) Nanostruct Mater 11:343
39. Ebrahimi F, Zhai Q, Kong D, Bourne GR (1999) In: Chung et al Y-W (eds) Advanced materials for 21st century: the 1999 Julia Weertman symposium. TMS Publication, Warrendale Pacific, p 421
40. Ebrahimi F, Ahmed Z, Li HQ (2006) Materials and manufacturing processes 21:687
41. Ma E (2006) JOM 58:49
42. ASM Handbook (1974) vol 9, 8th edn. ASM International, Ohio, p 72